Journal of Quantitative Spectroscopy & Radiative Transfer 170 (2016) 169–181

Contents lists available at ScienceDirect

Journal of Quantitative Spectroscopy & Radiative Transfer

journal homepage: www.elsevier.com/locate/jqsrt

Configuration interaction study on the ground and excited electronic states of the SrH molecule

Xiaoting Liu [a,b], Guiying Liang [a,b], Xiaomei Zhang [a,b], Haifeng Xu [a,b,*], Bing Yan [a,b,*]

[a] Institute of Atomic and Molecular Physics, Jilin University, Changchun 130012, China
[b] Jilin Provincial Key Laboratory of Applied Atomic and Molecular Spectroscopy, Jilin University, Changchun 130012, China

ARTICLE INFO

Article history:
Received 22 July 2015
Received in revised form
30 October 2015
Accepted 1 November 2015
Available online 18 November 2015

Keywords:
MRCI+Q
SrH
Spectroscopic constant
Radiative lifetimes

ABSTRACT

High-level *ab initio* calculations on the ground and the excited states of the SrH molecule have been carried out utilizing the multi-reference configuration interaction method plus Davidson correction (MRCI+Q) method, with small-core relativistic effective core potentials together with the corresponding correlation consistent polarized valence basis sets. The potential energy curves (PECs) of the 16 Λ–S states have been obtained with the aid of the avoided crossing rule between electronic states of the same symmetry. The spectroscopic constants of the bound states were calculated, most of which have been reported for the first time, with those pertaining to the $X^2\Sigma^+$, $A^2\Pi$, $B^2\Sigma^+$, and $A'^2\Delta$ states being in line with the available experimental and theoretical values. The calculated spin–orbit matrix element indicates a strong interaction between the $X^2\Sigma^+$ and $A^2\Pi$ states in the Franck–Condon region. The spin–orbit coupling (SOC) splits the lowest strongly bound $X^2\Sigma^+$, $A^2\Pi$, $A'^2\Delta$, $B^2\Sigma^+$, and $D^2\Sigma^+$ states into 9 Ω states. For the $D^2\Sigma^+$ state, the SOC shifts the potential-well minimum to higher energy and shortens the bond length. The transition properties of the bound Λ–S states were predicated, including the transition dipole moments (TDMs), the Franck–Condon factors, and the radiative lifetimes. The lifetimes were calculated to be 34.2 ns ($v'=0$) and 55.0 ns ($v'=0$) for $A^2\Pi$ and $B^2\Sigma^+$, in good agreement with the experimental results of 33.8 ± 1.9 ns and 48.4 ± 2.0 ns.

1. Introduction

Metal hydrides have attracted much attention due to their importance in many fields including astrochemistry, chemical process, and chemical engineering. The previous theoretical and experimental studies on metal hydride molecules were motivated by a variety of prospective applications [1–9]. The alkaline-earth metal hydrides are one category of them, which are exceedingly abundant in the sunspots, stars, nebulae, and the interstellar medium [10,11,12]. And therefore these species are expected to take part in chemical reactions in the interstellar medium. To model these reactions accurately information on the electronic structure and transition properties of abundant alkaline-hydrides is required. Therefore alkaline-earth metal hydrides have become the subject of numerous experimental and theoretical works [13–16]. Strontium monohydride (SrH) is easy to synthesize in the gas-phase and has been discovered on many stars, which has been reported in the literatures [17,18,19]. The astrophysical significance of the SrH molecule motivates us to perform the study on its electronic structure and transition properties.

SrH was first observed and characterized experimentally in the 1930s by Watson and Fredrickson [20]. Since that time there have been a number of experimental studies

* Corresponding authors at: Institute of Atomic and Molecular Physics, Jilin University, Changchun 130012, China.
E-mail addresses: xuhf@jlu.edu.cn (H. Xu), yanbing@jlu.edu.cn (B. Yan).

http://dx.doi.org/10.1016/j.jqsrt.2015.11.001
0022-4073/

identifying band systems spanning the ultraviolet–visible-near infrared regions of the spectrum. More recently Appelblad and Klynning recorded the high resolution spectra of $A^2\Pi$–$X^2\Sigma^+$ and $B^2\Sigma^+$–$X^2\Sigma^+$ band systems of SrH by using Fourier transform spectrophotometry [21]. Time-resolved experiments on the $A^2\Pi$–$X^2\Sigma^+$ transition were reported by Berg et al. [22], who determined the radiative lifetime of the $A^2\Pi_{1/2}$ ($\nu'=0$) state to be 33.8 ± 1.9 ns. Later, experiments by the same group [23] measured the lifetimes of the $\nu=0$ and 1 vibrational levels of the $A^2\Pi_{3/2}$ and $B^2\Sigma^+$ states. In 2004, Shayesteh et al. [24] measured the vibration–rotation spectra for $1\rightarrow0$ to $4\rightarrow3$ bands of SrH with a Fourier transform spectrometer. In 2012 Ram et al. [25] observed the high-resolution spectra of the $E^2\Pi\rightarrow X^2\Sigma^+$ transition of SrH and SrD by utilizing Fourier transform spectrometry, improving the existing set of spectroscopic constants for the $E^2\Pi$ state. In addition to determining spectroscopic constants of some low-lying states, previous experiments were able to deduce the type and magnitude of perturbations between the electronic states. For instance, in the 0–0 and 1–1 bands of the $E^2\Pi\rightarrow X^2\Sigma^+$ transition, the higher rotational levels of the $E^2\Pi$ state were found to be perturbed by another electronic state [25]. To further investigate the interactions between electronic states, a complete picture of potential energy curves of all low-lying states including different orbital and spin quantum numbers is required.

Theoretically there have been several studies reported on both the ground and low lying excited states of SrH. Leininger et al. [26] reported on the theoretical investigation of the four lowest excited electronic states of the SrH molecule, utilizing the configuration interaction method and small-core relativistic pseudopotentials, with the results indicating a double-well potential for the $B^2\Sigma^+$ state. More recently in 2014, Gao et al. [27] performed high-precision MRCI+Q calculations on the ground $X^2\Sigma^+$ state and the first excited $A^2\Pi$ state of SrH.

In all the previously reported experimental and theoretical work, only the lowest electronic states of SrH were investigated, with the relatively large discrepancies still existing between the reported theoretical and experimental results. Due to SrH having a high density of states in the Franck–Condon region strong interactions, e.g. via SOC, exist between the adjacent states. In this paper, we report on the further theoretical study on the low-lying Λ–S states of SrH with high level *ab initio* methods. Also calculations are the transition properties including the transition dipole moments, Franck–Condon factors and excited state lifetimes of the transitions. This is the first systematic *ab initio* study on PECs, dipole moments functions, and transition properties of the 16 Λ–S states correlating to the lowest five atomic dissociation limits for SrH. A complete picture for low-lying electronic states is presented through our computational work. The core–valence electrons correlations and relativistic effects are considered by high-level multi-reference method in combination with newly-developed large correlation-consistent basis set. Additionally, the present work provides theoretical comparisons with recent experimental results and a comparative study with further single-electron core-polarization potential investigations on electronic states of SrH.

2. Methods and computational details

Ab initio calculations were performed on the electronic structures SrH with the MOLPRO 2012 quantum chemistry program package [28,29].

Single point energy calculations on SrH were performed to obtain PECs. Based on the calculated PECs, spectroscopic constants of the bound excited electronic states were determined by solving the radial Schrödinger equation with the aid of the LEVEL program [30].

The adiabatic PECs of the ground state and excited states of SrH, were constructed from 79 single point energies corresponding to internuclear distances from 1.4 Å to 8.0 Å. In these calculations, the Gaussian-type contracted basis set cc-pwCV5Z-PP [31] with ECP28MDF [15] was selected for the Sr atom and uncontracted basis set aug-cc-pV5Z [32] for the H atom. The calculations were performed via the following three steps: the single-configuration wavefunction of the ground state for the SrH was firstly calculated with the restricted Hartree–Fock (RHF) method; then, the state-averaged complete active space self-consistent field (SA-CASSCF) method [33,34] was used to construct the multi-configuration wavefunction that could consider the degeneracy or near degeneracy of the states; finally, the internally contracted MRCI (icMRCI) approach was employed to treatment the dynamical correlation of the electrons. Adding the Davidson correction [35] (+Q) balances the size-consistency error of MRCI method. The PECs of these 16 Λ–S electronic states were drawn with the help of the avoided crossing rule of the states that have the same symmetry.

The symmetry point group of SrH is $C_{\infty v}$ point group. Due to a limitation of the MOLPRO program, the C_{2v} point group symmetry was chosen in the present calculation. The C_{2v} point group holds A1/B1/B2/A2 irreducible representations, and the corresponding relationships between the C_{2v} and $C_{\infty v}$ point group are $\Sigma^+=A_1$, $\Pi=B_1+B_2$, $\Delta=A_1+A_2$, and $\Sigma^-=A_2$. For the SrH, $6a_1$, $2b_1$, $2b_2$, and $1a_2$ symmetry molecular orbitals (MOs) were determined as the active space, corresponding to the atomic orbitals 4s4p5s5p4d6s for Sr and 1s for H. The outermost $5s^2$ electrons of the Sr atom and $1s^1$ electron of the H atom were placed in the active space. The rest of the electrons for Sr, which were semicore electrons of 4s and 4p, were placed in the closed shell. These orbitals are doubly occupied in all reference configuration state functions, and correlated via single and double excitations. That is, there were total of 11 electrons of the SrH used in the calculation of electronic correlation energy.

Based on the PECs of the Λ–S, the spectroscopic constants, including equilibrium internuclear distance R_e, excitation energy T_e, vibrational constants ω_e and $\omega_e x_e$, rotation constant B_e, and vibrational–rotational coupling constant α_e, were determined by numerical solution of the one-dimensional nuclear Schrödinger equation. The dissociation energy D_e was obtained by subtracting the molecular energy at R_e from the energy at a large separation. The transition properties of the SrH radical were predicted. The spin–orbit matrix elements of the lowest electronic states were calculated at the CASSCF level, while the TDMs and the permanent dipole moments were evaluated at the icMRCI level. The *ab initio* grid points data of all the curves for Λ–S states, Ω state, TDMs, and dipole

moments are presented in the supplementary material. The Franck–Condon factors were calculated with the aid of the LEVEL program [30]. Based on the calculated TDMs and Franck–Condon factors, the radiative lifetimes for several of the lowest energy transitions were predicted.

3. Results and discussion

3.1. The PECs and the spectroscopic constants of the Λ–S states

The 16 Λ–S states of SrH, associated with five dissociation limits of $Sr(^1S_g)+H(^2S_g)$, $Sr(^3P_g)+H(^2S_g)$, $Sr(^3D_g)+H(^2S_g)$, $Sr(^1D_g)+H(^2S_g)$, and $Sr(^1P_u)+H(^2S_g)$, have been calculated with the MRCI+Q method. The detailed dissociation relationships of the electronic states are listed in Table 1. The corresponding energy gaps of the ^3P_u–^1S_g, ^3D_g–^1S_g, ^1D_g–^1S_g and ^1P_u–^1S_g levels of the Sr atom are computed to be 1.80, 2.32, 2.57, 2.75 eV, which are in good agreement with the experimental values of 1.82, 2.26, 2.50, 2.69eV with errors of less than 0.1 eV [36].

Table 1
The dissociation relationships of the Λ–S states.

Λ–S states	Atomic state	Energy (eV)	
	(Sr+H)	Calc.	Expt.[a]
$X^2\Sigma^+$	$(5s^2)^1S_g+(1s)^2S_g$	0	0
$A^2\Pi$, $B^2\Sigma^+$, $^4\Sigma^+(1)$, $^4\Pi(1)$	$(5s5p)^3P_u+(1s)^2S_g$	1.80	1.82
$D^2\Sigma^+$, $E^2\Pi$, $^4\Sigma^+(2)$, $^4\Pi(2)$, $A'^2\Delta$, $^4\Delta$	$(5s4d)^3D_g+(1s)^2S_g$	2.32	2.26
$C^2\Sigma^+$, $^2\Pi(3)$, $^2\Delta(2)$	$(5s4d)^1D_g+(1s)^2S_g$	2.57	2.50
$F^2\Sigma^+$, $^2\Pi(4)$	$(5s5p)^1P_u+(1s)^2S_g$	2.75	2.69

[a] Ref. [36].

These test calculations show that the inclusion of semicore–valence electrons correlations is vital to obtain correct relative energies for excited states of the Sr atom. The determined PECs of the Λ–S states are plotted in Fig. 1. From these calculated PECs, it is found that 10 of the 16 calculated excited states correspond to bound states. By solving the nuclear Schrödinger equation, the spectroscopic constants of the bound states are determined and listed in Table 2. In order to show the multi-configuration characteristic of each bound states, the electronic configurations around the equilibrium internuclear distances (R_e) are also given in Table 2.

Since effective core potential (ECP) is used in this work, the $n=1$–3 shells of Sr atom corresponding to 1–6σ, 1–3π and 1δ molecular orbitals are not included in computations, while still counted into the number of molecular orbitals for clarity. The 7σ and 8σ+4π corresponding to 4s and 4p atomic orbitals of Sr are kept doubly occupied in CASSCF computations. As listed in Table 2, the ground state $X^2\Sigma^+$ is mainly from the electronic configuration $9\sigma^2 10\sigma^{\alpha} 11\sigma^0 12\sigma^0 13\sigma^0 5\pi^0 6\pi^0 2\delta^0$ with a small account of mixtures from 9σ–10σ and 10σ–11σ transitions. In the electronic configuration, the binding 7σ and 8σ orbital corresponds to a linear combination of the 5s orbital for Sr and 1s orbital for H, and other molecular orbitals correspond to 5pσ(Sr), 4dσ(Sr), 6sσ(Sr), 5pπ(Sr), 4dπ(Sr) and 4dδ(Sr) molecular orbitals, respectively. As listed in Table 2, our computed spectroscopic constants with MRCI+Q method excellently reproduce the observed values [21,24,37]. The deviations are only 0.003 Å, 13.12 cm^{-1}, 1.4 cm^{-1}, 6 cm^{-1} and 0.018 eV for R_e, ω_e, $\omega_e x_e$, B_e, and D_e, respectively. Our results are also close to the recent theoretical values calculated by Gao et al. [27]. The first excited state $A^2\Pi$ arises from the electronic configurations $9\sigma^2 5\pi^{\alpha}$ (48.8%) and $9\sigma^2 6\pi^{\alpha}$ (31.5%), corresponding to a single-electron transition from the 1s of the H atom to the 5p and 4d of Sr. Our results of R_e

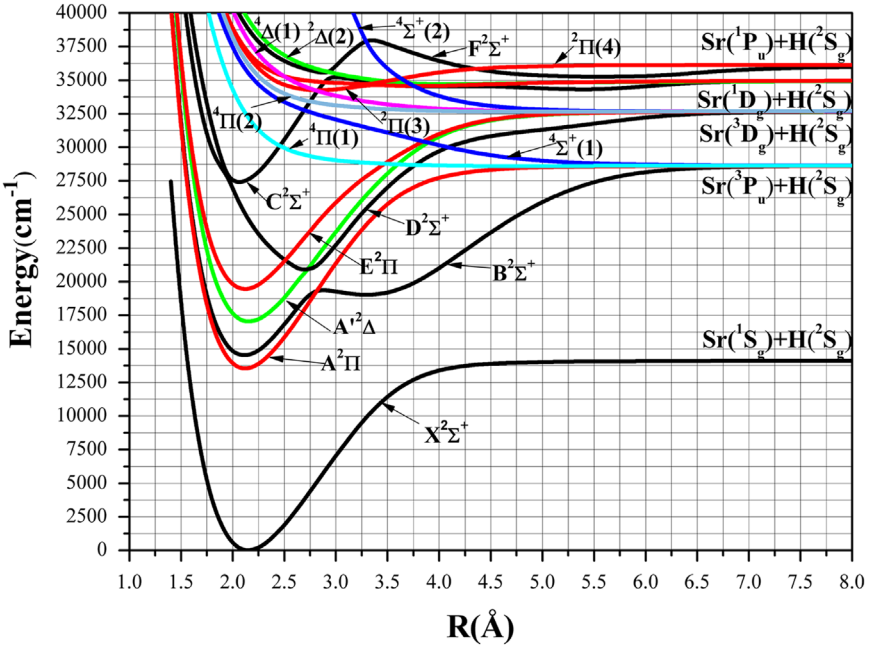

Fig. 1. The PECs of the Λ–S states.

Table 2
The spectroscopic constants of the Λ–S states.

Λ–S State	T_e(cm^{-1})	R_e(Å)	ω_e(cm^{-1})	$\omega_e x_e$(cm^{-1})	B_e(cm^{-1})	$10^2\alpha_e$(cm^{-1})	D_e(eV)	Main configurations at R_e (%)
$X^2\Sigma^+$	0	2.149	1219.32	18.400	3.669	8.382	1.750	$9\sigma^2 10\sigma^\alpha 11\sigma^0 12\sigma^0 13\sigma^0 5\pi^0 6\pi^0 2\delta^0$ (79.4) $9\sigma^\alpha 10\sigma^2 11\sigma^0 12\sigma^0 13\sigma^0 5\pi^0 6\pi^0 2\delta^0$ (3.3) $9\sigma^2 10\sigma^0 11\sigma^\alpha 12\sigma^0 13\sigma^0 5\pi^0 6\pi^0 2\delta^0$ (3.2)
Expt.	0[a]	2.146[a,b,c]	1206.2[a]/1207.0[b,c]	17.0[a]/17.2[b]/17.1[c]	3.675[a]/3.674[b,c]	8.14[a]/8.023[c]	1.732[a]/1.678[c]	
Calc.	0	2.143[d]/2.211[e]/2.21[f]	1222.88[d]/1166.2[e]/1167[f]	18.4[d]/19[f]	3.684[d]/3.45[e]/3.43[f]		1.768[d]/1.470[f]	
$A^2\Pi$	13525	2.119	1272.09	19.486	3.770	14.913	1.871	$9\sigma^2 10\sigma^0 11\sigma^0 12\sigma^0 13\sigma^0 5\pi^\alpha 6\pi^0 2\delta^0$ (48.8) $9\sigma^2 10\sigma^0 11\sigma^0 12\sigma^0 13\sigma^0 5\pi^0 6\pi^\alpha 2\delta^0$ (31.5) $9\sigma^\alpha 10\sigma^\beta 11\sigma^0 12\sigma^0 13\sigma^0 5\pi^\alpha 6\pi^0 2\delta^0$ (5.1) $9\sigma^\alpha 10\sigma^0 11\sigma^0 12\sigma^0 13\sigma^\alpha 5\pi^\alpha 6\pi^0 2\delta^0$ (2.8)
Expt.	13500[c]	2.148[a]/2.121[c]	1253.9[c]	18.0[c]	3.668[a]/3.75[c]			
Calc.	13487[d]/13112[e]	2.109[d]/2.172[e]	1273.03[d]/1214.5[e]	17.7[d]	3.805[d]/3.58[e]		1.887[d]	
$B^2\Sigma^+$								
1st well	14503	2.113	1217.78	20.105	3.799	9.40	1.751	$9\sigma^2 10\sigma^0 11\sigma^\alpha 12\sigma^0 13\sigma^0 5\pi^0 6\pi^0 2\delta^0$ (73.8) $9\sigma^\alpha 10\sigma^\beta 11\sigma^\alpha 12\sigma^0 13\sigma^0 5\pi^0 6\pi^0 2\delta^0$ (7.6) $9\sigma^\alpha 10\sigma^0 11\sigma^\alpha 12\sigma^0 13\sigma^\beta 5\pi^0 6\pi^0 2\delta^0$ (2.9)
Expt.	14340[a]/14313[c]	2.089[a]/2.117[c]	1193.0[a]/1234.34[c]	19[a]/21.132[c]	3.879[a]/3.775[c]	9.30[a]	1.731[a]/1.741[c]	
Calc.	14734[e]/14952[f]	2.160[e]/2.20[f]	1192[e]/1288[f]	31[f]	3.62[e]/3.47[f]	7.940[f]	1.420[f]	
2nd well	19024	3.296	721.563($\Delta G_{1/2}$)		1.565(B_0)		1.191	$9\sigma^\alpha 10\sigma^2 11\sigma^0 12\sigma^0 13\sigma^0 5\pi^0 6\pi^0 2\delta^0$ (55.1) $9\sigma^2 10\sigma^\alpha 11\sigma^0 12\sigma^0 13\sigma^0 5\pi^0 6\pi^0 2\delta^0$ (16.5) $9\sigma^\alpha 10\sigma^\beta 11\sigma^\beta 12\sigma^0 13\sigma^0 5\pi^0 6\pi^0 2\delta^0$ (6.0)
$A'^2\Delta$	17027	2.153	1198.249	18.598	3.645	6.908	1.939	$9\sigma^2 10\sigma^0 11\sigma^0 12\sigma^0 13\sigma^0 5\pi^0 6\pi^0 2\delta^\alpha$ (78.6) $9\sigma^\alpha 10\sigma^\beta 11\sigma^0 12\sigma^0 13\sigma^0 5\pi^0 6\pi^0 2\delta^\alpha$ (7.6) $9\sigma^\alpha 10\sigma^0 11\sigma^0 12\sigma^0 13\sigma^\beta 5\pi^0 6\pi^0 2\delta^\alpha$ (4.6)
$E^2\Pi$	19449	2.117	1229.806	27.658	3.774	14.913	1.641	$9\sigma^2 10\sigma^0 11\sigma^0 12\sigma^0 13\sigma^0 5\pi^0 6\pi^\alpha 2\delta^0$ (43.1) $9\sigma^2 10\sigma^0 11\sigma^0 12\sigma^0 13\sigma^0 5\pi^\alpha 6\pi^0 2\delta^0$ (23.3) $9\sigma^\alpha 10\sigma^\beta 11\sigma^0 12\sigma^0 13\sigma^0 5\pi^0 6\pi^\alpha 2\delta^0$ (9.7) $9\sigma^2 10\sigma^\beta 11\sigma^0 12\sigma^0 13\sigma^0 5\pi^\alpha 6\pi^0 2\delta^0$ (8.8)
Expt.		2.1083727(89)[g]/2.156[a]			3.805503(32)[g]/3.639[a]	9.8880(47)[g]		
$D^2\Sigma^+$	20915	2.697	1121.00	28.866	2.314		1.458	$9\sigma^\alpha 10\sigma^2 11\sigma^0 12\sigma^0 13\sigma^0 5\pi^0 6\pi^0 2\delta^0$ (51.5) $9\sigma^2 10\sigma^0 11\sigma^\alpha 12\sigma^0 13\sigma^0 5\pi^0 6\pi^0 2\delta^0$ (17.4) $9\sigma^2 10\sigma^\alpha 11\sigma^0 12\sigma^0 13\sigma^0 5\pi^0 6\pi^0 2\delta^0$ (7.7) $9\sigma^2 10\sigma^0 11\sigma^0 12\sigma^0 13\sigma^\alpha 5\pi^0 6\pi^0 2\delta^0$ (2.4) $9\sigma^\alpha 10\sigma^\beta 11\sigma^0 12\sigma^0 13\sigma^\alpha 5\pi^0 6\pi^0 2\delta^0$ (2.3)
Expt.	20847.6[a]	2.965[a]	1014.1[a]	15.4[a]	1.925[a]	2.4[a]		
Calc.			1347[h]	23.5[h]	4.008[h]			
$C^2\Sigma^+$	27391	2.063	1471.59	35.094	3.987	15.84	0.933	$9\sigma^2 10\sigma^0 11\sigma^0 12\sigma^\alpha 13\sigma^0 5\pi^0 6\pi^0 2\delta^0$ (76.0) $9\sigma^\alpha 10\sigma^\beta 11\sigma^0 12\sigma^\alpha 13\sigma^0 5\pi^0 6\pi^0 2\delta^0$ (7.8) $9\sigma^\alpha 10\sigma^0 11\sigma^0 12\sigma^\alpha 13\sigma^\beta 5\pi^0 6\pi^0 2\delta^0$ (3.7)
Expt.	26230[a]	2.055[a]	1347[a]	23.5[a]	4.008[a]	13.2[a]		
Calc.			1014.1[h]	15.4[h]	1.925[h]			
$^2\Pi(3)$	34253	2.8325	233.650	22.938	2.416	—	0.087	$9\sigma^2 10\sigma^\alpha 11\sigma^0 12\sigma^0 13\sigma^0 5\pi^\beta 6\pi^0 2\delta^0$ (59.7) $9\sigma^2 10\sigma^\beta 11\sigma^0 12\sigma^0 13\sigma^0 5\pi^\alpha 6\pi^0 2\delta^0$ (19.4) $9\sigma^\alpha 10\sigma^\beta 11\sigma^0 12\sigma^0 13\sigma^0 5\pi^0 6\pi^\alpha 2\delta^0$ (10.9) $9\sigma^2 10\sigma^0 11\sigma^0 12\sigma^0 13\sigma^0 5\pi^\alpha 6\pi^0 2\delta^0$ (8.5)
$^2\Pi(4)$	34724	3.271	381.068	23.056	1.678	—	0.175	$9\sigma^2 10\sigma^\beta 11\sigma^0 12\sigma^0 13\sigma^0 5\pi^0 6\pi^\alpha 2\delta^0$ (56.3) $9\sigma^\alpha 10\sigma^\beta 11\sigma^0 12\sigma^0 13\sigma^0 5\pi^\alpha 6\pi^0 2\delta^0$ (19.6) $9\sigma^\alpha 10\sigma^0 11\sigma^\alpha 12\sigma^0 13\sigma^0 5\pi^\beta 6\pi^0 2\delta^0$ (5.7) $9\sigma^\alpha 10\sigma^\beta 11\sigma^0 12\sigma^0 13\sigma^0 5\pi^\alpha 6\pi^0 2\delta^0$ (4.7)

$F^2\Sigma^+$	35263	5.5715	153.60	2.2105	0.5462	–	0.088	$9\sigma^{\alpha}10\sigma^{\alpha}11\sigma^{b}12\sigma^{0}13\sigma^{0}5\pi^{0}6\pi^{0}2\delta^{0}$ (49.4) $9\sigma^{\alpha}10\sigma^{b}11\sigma^{\alpha}12\sigma^{0}13\sigma^{0}5\pi^{0}6\pi^{0}2\delta^{0}$ (14.0) $9\sigma^{2}10\sigma^{0}11\sigma^{0}12\sigma^{\alpha}13\sigma^{0}5\pi^{0}6\pi^{0}2\delta^{0}$ (7.5) $9\sigma^{\alpha}10\sigma^{b}11\sigma^{0}12\sigma^{\alpha}13\sigma^{0}5\pi^{0}6\pi^{0}2\delta^{0}$ (4.2) $9\sigma^{2}10\sigma^{0}11\sigma^{\alpha}12\sigma^{0}13\sigma^{0}5\pi^{0}6\pi^{0}2\delta^{0}$ (3.3)

[a] Ref [37].
[b] Ref [24].
[c] Ref [21].
[d] Ref [27].
[e] Ref [38].
[f] Ref [26].
[g] Ref [25].
[h] Ref [39].

and B_e are 2.119 Å and 3.770 cm^{-1} which are more close to the experimental values [37] of 2.148 Å and 3.668 cm^{-1} than recent theoretical values of 2.109 Å and 3.805 cm^{-1} [27]. This state lies 13,525 cm^{-1} above ground state with equilibrium internuclear distance at R_e=2.119 Å.

The $B^2\Sigma^+$ state is calculated to be energetically close to $A^2\Pi$ state with an energy gap of 978 cm^{-1}, leading to the possibility of strong interactions existing between them. The other remarkable characteristic is the calculated double-well potential of the $B^2\Sigma^+$ state in agreement with previous calculations [26]. The spectroscopic constants of the two potential wells are determined and listed in Table 2. The inner well is located at R=2.113 Å and the outer one at R=3.296 Å. The double well nature of the PEC is due to an avoided crossing with the $D^2\Sigma^+$ state. This interaction further results in the $D^2\Sigma^+$ state having a larger calculated equilibrium internuclear distance. The other two electronic states $A'^2\Delta$ and $E^2\Pi$ have similar calculated bond lengths and are both strongly bound. The dissociation energies D_e and excitation energies T_e are calculated to be 2.153 eV, 17,027 cm^{-1} for the $A'^2\Delta$ state and 2.117 eV, 19,449 cm^{-1} for the $E^2\Pi$ state. And the experimental results of the r_e and B_e for the $E^2\Pi$ state are 2.156 Å and 3.639 cm^{-1} [37], respectively. Our computed values are 2.117 Å and 3.774 cm^{-1}, which are in reasonable agreement with the existing experimental results [37]. For the $D^2\Sigma^+$ state, our calculated values of the T_e, r_e, ω_e and B_e are in good accordance with the existing experimental results [37]. The adiabatic excitation energies of the four excited electronic states $A^2\Pi$, $A'^2\Delta$, $B^2\Sigma^+$, and $E^2\Pi$ indicate that these electronic states are very close in energy to each other. Therefore, strong interactions induced by SOC are present among these states, and will be discussed in detail in the next section. The remaining electronic states correlating to the Sr (^3D_g)+H(^2S_g) are all typically repulsive over the internuclear distance. The higher electronic state $C^2\Sigma^+$ is found to have an avoided crossing with the $D^2\Sigma^+$ state around the well bottom (2 Å) and with the $F^2\Sigma^+$ state at the longer distance about 3 Å. Similarly, the weakly bound $^2\Pi(3)$ and $^2\Pi(4)$ states also have an avoided crossing at a bond length about 3.5 Å. The two states are separately correlated to two adjacent dissociation limits Sr(^1P_u)+H(^2S_g) and Sr(^1D_g)+H(^2S_g) with the small energy interval of 0.18 eV.

For these Λ–S states, the permanent dipole moments (PDMs) of the ten bound states are also calculated as the function of the internuclear distance and the curves are plotted in Fig. 2. Fig. 2 also shows the curves of PDMs reported in the previous work for comparison. As shown in the figure, all the calculated dipole moments tend to zero at large distance, confirming that the dissociation products are both neutral atoms. For the ground state $X^2\Sigma^+$, the PDM curve is close to that determined by Leininger et al. [26]. Our calculated PDM curve of the $A^2\Pi$ state is similar to PDM curve that has been recently calculated by Gao et al. [27], while about two times smaller than that calculated by Leininger et al. [26], with the calculated trend with increasing R in the three works being similar. Leininger et al. also calculated the PDMs of the $B^2\Sigma^+$ and $A'^2\Delta$ states; though differences between the current and Leininger's calculations still can be observed in Fig. 2, a similar trend is found especially for large internuclear distance. The sudden complementary

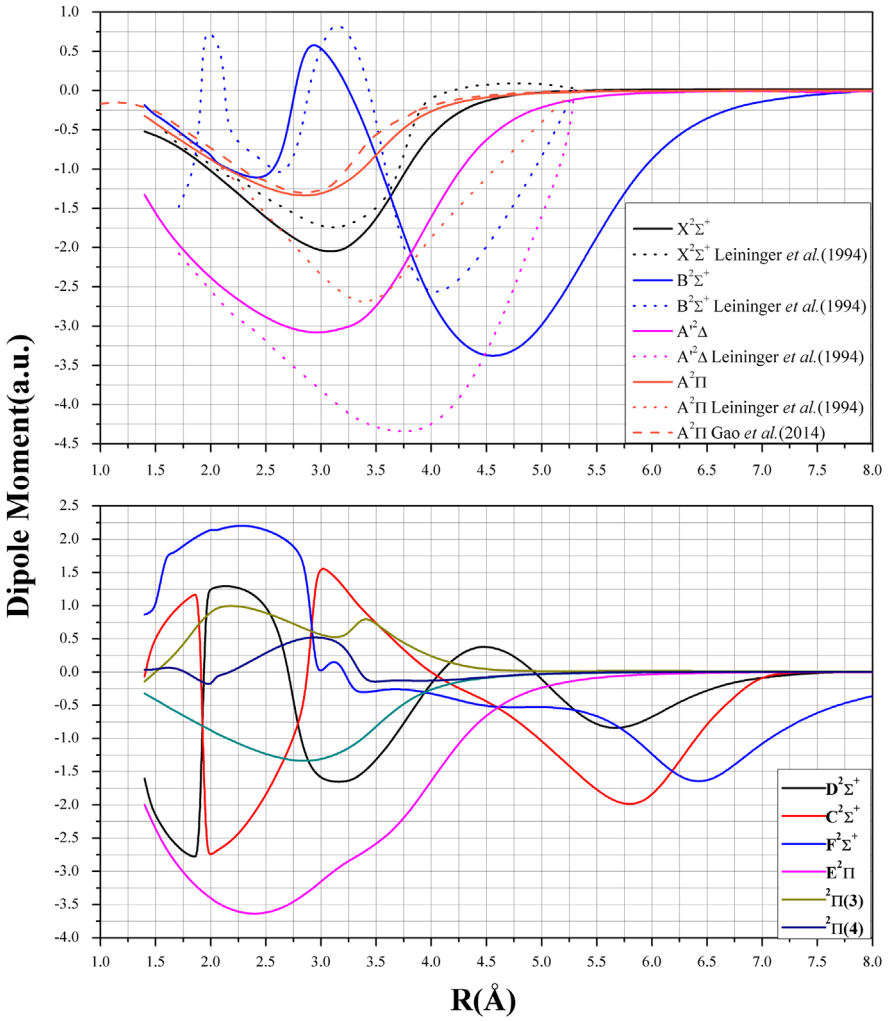

Fig. 2. The permanent dipole moments of the bound states for the SrH molecule.

changes for the dipole moments of the $D^2\Sigma^+$ and $C^2\Sigma^+$ states at about $R=2$ Å, and between the $C^2\Sigma^+$ and $F^2\Sigma^+$ states at longer distance of about $R=3$ Å are due to the avoided crossings mentioned above. In addition, the dipole moment of the $F^2\Sigma^+$ state tends to zero at a slower speed, which indicates the Rydberg characteristic of the $F^2\Sigma^+$ state. This is due to the electron excitations to 11σ and 12σ orbitals that are associated with the higher-energy atomic 5p and 4d orbitals of Sr. It is proposed here that the $F^2\Sigma^+$ state dissociates to a higher Rydberg state which has the same $^2\Sigma^+$ symmetry whose PEC crosses that of the $F^2\Sigma^+$ state and dissociates to the $Sr(^1P_g)+H(^2S_g)$ state. Due to the two states having the same symmetry they must abide by the avoided crossing rule between states of the same symmetry, as in the case of BBr which has been studied by Yang and Boggs [40].

3.2. The spin–orbit coupling effect on the SrH radical

As discussed above, a density of high electronic states has been calculated for SrH, with most of the states having deep potential wells (> 1 eV). Thus with the notation that SOC may exist between the states; the interaction strength is studied via the magnitude of spin–orbit matrix element. The SO matrix elements are calculated as a function of the internuclear distance. The corresponding curves are plotted in Fig. 3. And the SO operator can be represented in the basis of the real spin-electronic functions labeled as |term > , as in the case of CaO which has been studied by Khalil et al. [41].

$$SO_1 = -i < X^2\Sigma^+ \left| H_{SO}^{BP} \right| A^2\Pi_y >_x$$

$$SO_2 = -i < B^2\Sigma^+ \left| H_{SO}^{BP} \right| A^2\Pi_y >_x$$

$$SO_3 = -i < A'^2\Delta_x \left| H_{SO}^{BP} \right| A^2\Pi_y >_x$$

$$SO_4 = -i < D^2\Sigma^+ \left| H_{SO}^{BP} \right| A^2\Pi_y >_x$$

$$SO_5 = -i < X^2\Sigma^+ \left| H_{SO}^{BP} \right| E^2\Pi_y >_x$$

$$SO_6 = -i < B^2\Sigma^+ \left| H_{SO}^{BP} \right| E^2\Pi_y >_x$$

$$SO_7 = -i < A'^2\Delta_x \left| H_{SO}^{BP} \right| E^2\Pi_y >_x$$

$$SO_8 = -i < D^2\Sigma^+ \left| H_{SO}^{BP} \right| E^2\Pi_y >_x$$

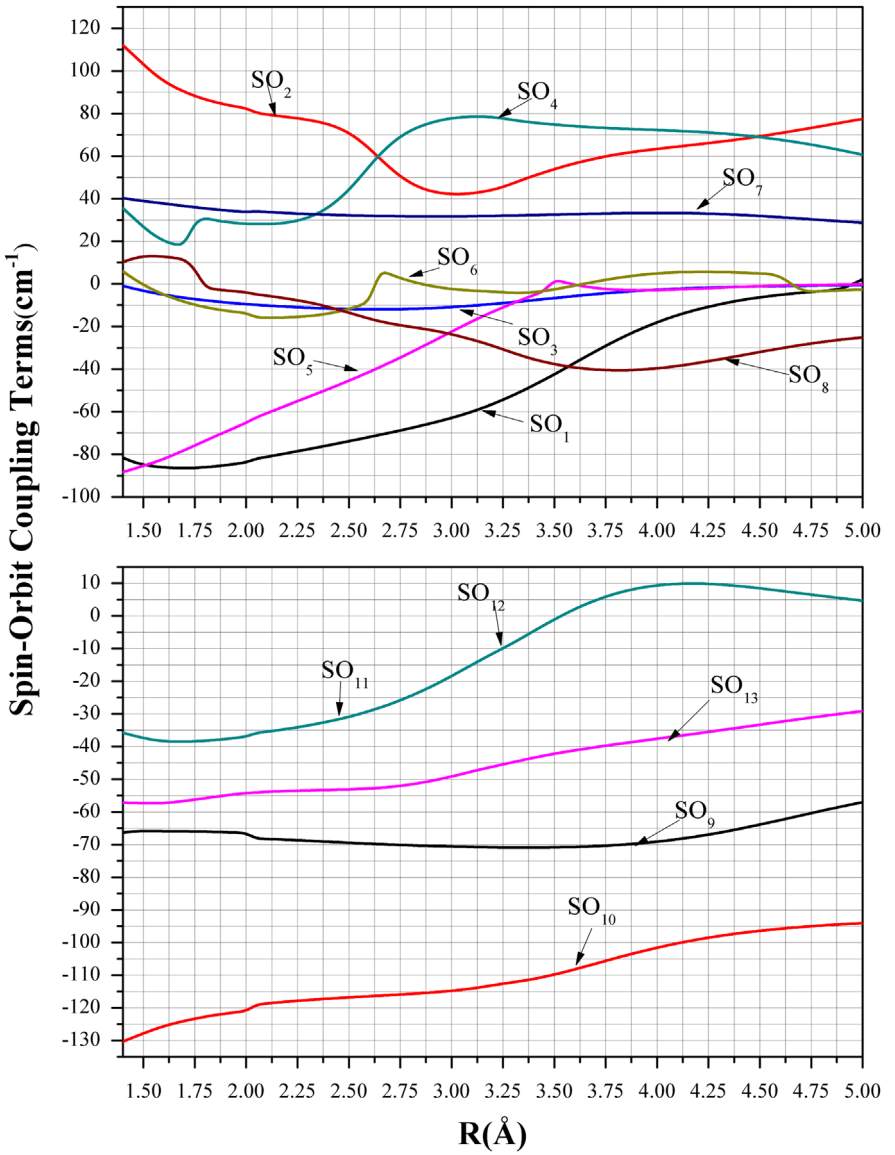

Fig. 3. The spin-orbit matrix elements of the lowest several Λ–S states. See Eq.(1) for the meaning of the different SO_i symbols.

$$
\begin{aligned}
SO_9 &= -i\langle A'^2\Delta_x \left| H_{SO}^{BP} \right| A'^2\Delta_y \rangle_z \\
SO_{10} &= -i\langle A^2\Pi_x \left| H_{SO}^{BP} \right| A^2\Pi_y \rangle_z \\
SO_{11} &= -i\langle E^2\Pi_x \left| H_{SO}^{BP} \right| A^2\Pi_y \rangle_z \\
SO_{12} &= -i\langle A^2\Pi_x \left| H_{SO}^{BP} \right| E^2\Pi_y \rangle_z \\
SO_{13} &= -i\langle E^2\Pi_x \left| H_{SO}^{BP} \right| E^2\Pi_y \rangle_z
\end{aligned} \tag{1}
$$

As shown in the figure, it was found that the matrix element of the $A^2\Pi$–$X^2\Sigma^+$ system has larger value of about $-80\ cm^{-1}$ in the Franck–Condon region, indicating a strong SO interaction between the $A^2\Pi$ and $X^2\Sigma^+$ states. The matrix elements of the $B^2\Sigma^+$–$A^2\Pi$ and $D^2\Sigma^+$–$A^2\Pi$ systems exhibit complementary trends between 2.5 and 3 Å for the reason of the afore mentioned avoided crossing between the $B^2\Sigma^+$ and $D^2\Sigma^+$ states in this region. The matrix element of the $E^2\Pi$–$X^2\Sigma^+$ reduces quickly as the internuclear distance increases. In contrast, with increasing bond length, the matrix element of the $E^2\Pi$–$A'^2\Delta$ system almost keeps the constant about $40\ cm^{-1}$, indicating the weaker interaction induced by the SOC between the $E^2\Pi$ and $A'^2\Delta$ states. Both Π states associated with the same configuration $SO_{11}=SO_{12}$ which is confirmed in Fig. 3.

The SOC also makes the six strongly bound states, i.e., the $X^2\Sigma^+$, $A^2\Pi$, $A'^2\Delta$, $E^2\Pi$, $B^2\Sigma^+$ and $D^2\Sigma^+$, split into 9 Ω states, including five $\Omega=1/2$, three $\Omega=3/2$, and one $\Omega=5/2$. The corresponding PECs of the Ω states are plotted in Fig. 4. The spectroscopic constants are determined and listed in Table 3 along with the main Λ–S compositions at R_e.

The ground $\Omega=1/2$ state completely consists of the $X^2\Sigma^+$ state in the Franck–Condon region. Therefore, the

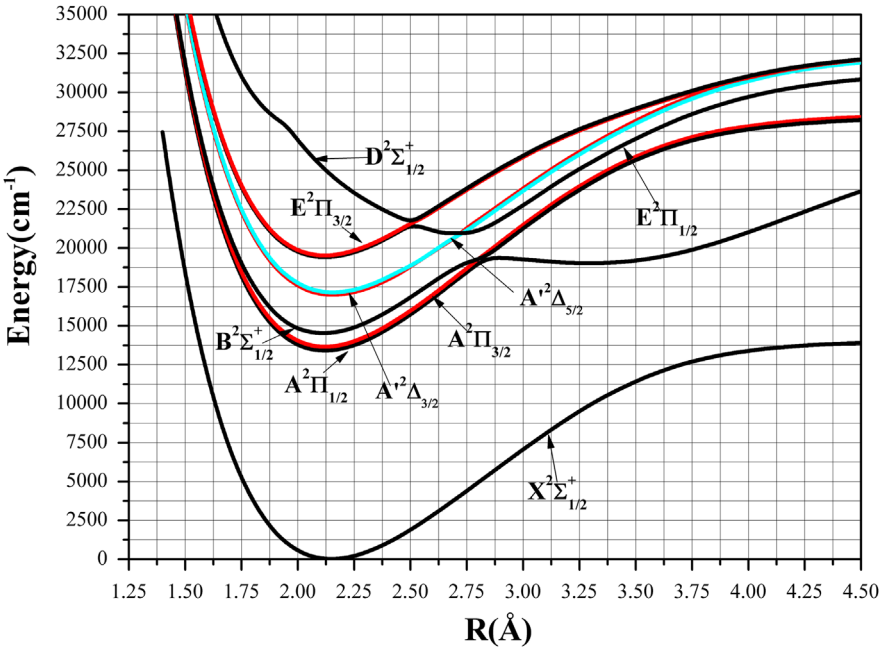

Fig. 4. The PECs of the Ω states.

Table 3
The spectroscopic constants of the Ω states.

Ω state	T_e (cm^{-1})	R_e (Å)	ω_e (cm^{-1})	$\omega_e x_e$ (cm^{-1})	B_e (cm^{-1})	$10^2\alpha_e$ (cm^{-1})	Main Λ–S components at R_e (%)
$X^2\Sigma^+_{1/2}$	0	2.1479	1208.22	18.399	3.668	8.034	$X^2\Sigma^+$(99.99)
Expt.	0[a]	2.146[a]	1206.2[a]	17.0[a]	3.675[a]	8.14[a]	
Calc.	0[b,c]	2.1458[b]/2.1456[c]	1232.56[b]/1206.2[c]	19.08[b]/17.0[c]	3.6753[b]/3.6751[c]		
$A^2\Pi_{1/2}$	13395.41	2.1179	1260.50	18.175	3.770	8.163	$A^2\Pi$(98.96), $B^2\Sigma^+$(1.03)
Calc.	12569.38[b]/13571[c]	2.1092[b]/2.16[c]	1309.81[b]/1175[c]	20.60[b]/14[c]	3.8052[b]/3.52[c]		
$A^2\Pi_{3/2}$	13643.42	2.1180	1263.49	19.512	3.769	8.264	$A^2\Pi$(99.98)
Expt.		2.148[a]			3.668[a]		
Calc.	12871.04[b]/13804[c]	2.1086[b]/2.16[c]	1311.08[b]/1173[c]	20.58[b]/13[c]	3.8074[b]/3.57[c]		
$B^2\Sigma^+_{1/2}$	14514.08	2.1125	1236.49	15.452	3.793	7.576	$B^2\Sigma^+$(98.97), $A^2\Pi$(1.02)
$A'^2\Delta_{3/2}$	16980.53	2.1534	1194.58	18.458	3.644	8.072	$A'^2\Delta$(99.93)
Calc.	16776[d]	2.19[d]	1044[d]		3.46[d]		
$A'^2\Delta_{5/2}$	17134.16	2.1533	1194.48	20.942	3.649	9.332	$A'^2\Delta$(100)
Calc.	16851[d]	2.17[d]	1043[d]		3.46[d]		
$E^2\Pi_{1/2}$							
1st well	19396.95	2.1174	1223.44	11.393	3.770	7.7347	$E^2\Pi$(100)
2nd well	20926.03	2.6617	1185.09	–	14.0965	–	$D^2\Sigma^+$(100)
$E^2\Pi_{3/2}$	19505.81	2.1186	1209.12	19.1986	3.769	9.063	$E^2\Pi$(99.92)
$D^2\Sigma^+_{1/2}$	21672.90	2.4988	2170.39	–	2.696	12.506	$D^2\Sigma^+$(80.95), $E^2\Pi$(19.02)

[a] Ref [37].
[b] Ref [27].
[c] Ref [26].
[d] Ref [21].

spectroscopic constants are almost the same as those of the $X^2\Sigma^+$ state. Nevertheless, comparing to experiment, the vibrational constant ω_e is improved, and the corresponding deviation from experiment reduces from 13 cm^{-1} to 2 cm^{-1}. The first excited state $A^2\Pi$ splits into the two states $\Omega=1/2$ and 3/2. At the equilibrium position, the energy interval is calculated to be 248 cm^{-1}, in good agreement with the previous theoretical values of 233 cm^{-1} [26] and 301.66 cm^{-1} [27], and in accordance with the experimental data of 290.157 cm^{-1} [21]. It can be seen from Fig. 4, as R increases, there is an avoided crossing between the $A^2\Pi_{1/2}$ and $B^2\Sigma^+_{1/2}$ states due to their common $\Omega=1/2$ value at about 2.8 Å. For the $A^2\Pi_{3/2}$ state, because there is no interaction with another $\Omega=3/2$ state, the shape of the PEC is the same as that of the $A^2\Pi$. The 5/2 and 3/2 Ω states generated from the $A'^2\Delta$ state almost keep unchanged, because of no common Ω component between the crossed $A'^2\Delta$ and $D^2\Sigma^+$ states. Due to the avoided crossing between the $D^2\Sigma^+_{1/2}$ and

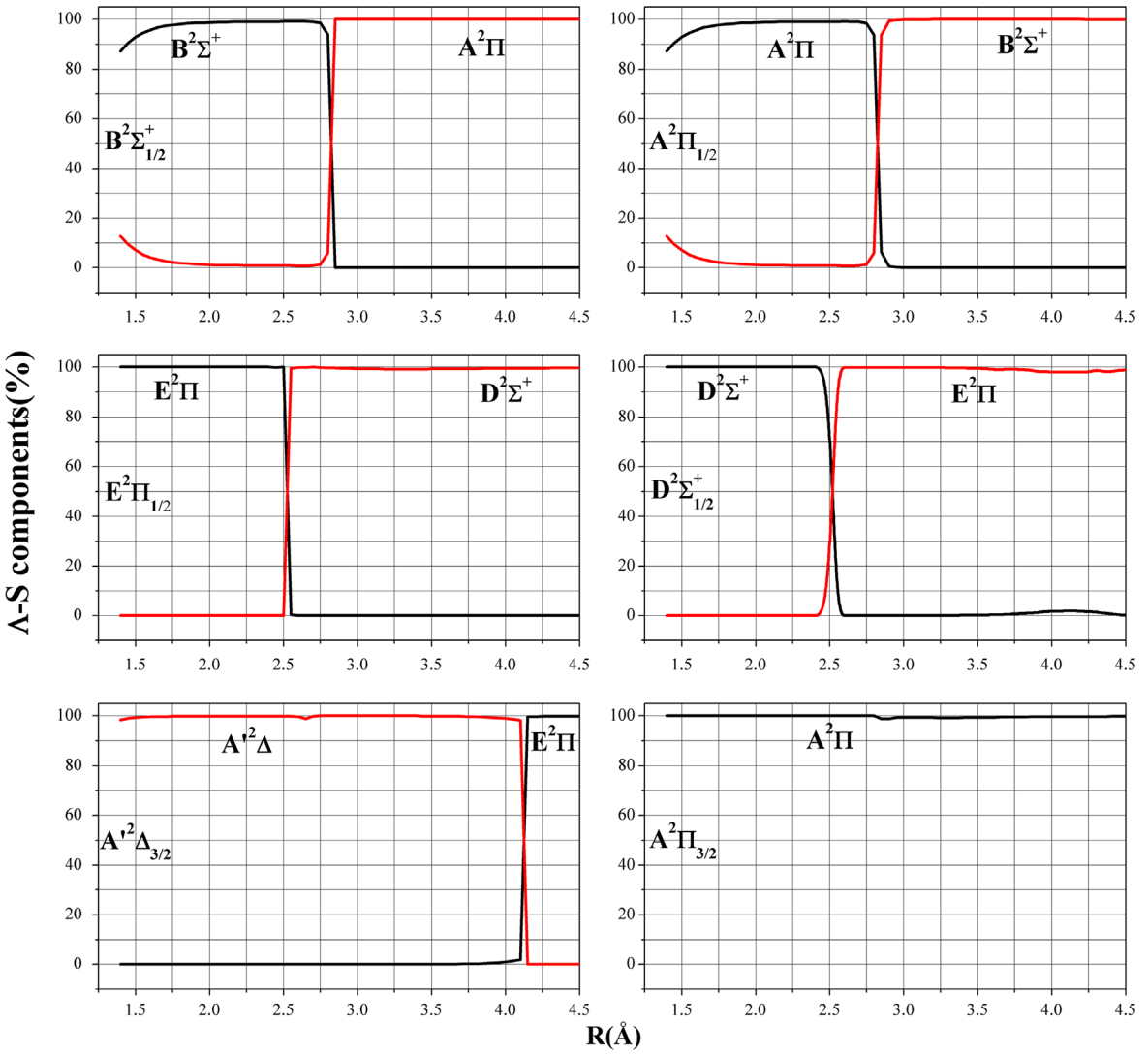

Fig. 5. The Λ–S compositions for the $A^2\Pi_{1/2}$, $A^2\Pi_{3/2}$, $B^2\Sigma^+_{1/2}$, $D^2\Sigma^+_{1/2}$, $E^2\Pi_{1/2}$, and $E^2\Pi_{3/2}$.

$E^2\Pi_{1/2}$ PECs, the $D^2\Sigma^+$ state potential well shifts higher in energy and the bond length shortens by 806 cm^{-1} and 0.1872 Å respectively, while a double-well potential results for the $E^2\Pi_{1/2}$ state. The calculated avoided crossings are also evident in the sharp changes observed in the Λ–S compositions. Fig. 5 shows the *R*-dependent Λ–S compositions of the $\Omega=1/2$ and 3/2 states. For the $A^2\Pi_{1/2}$ and $E^2\Pi_{1/2}$ states, the Λ–S compositions switch between the $A^2\Pi$ and $B^2\Sigma^+$ states and the $E^2\Pi$ and $D^2\Sigma^+$ states respectively at their respective avoided crossing points. In contrast, the $\Omega=3/2$ states fully consist of the $A^2\Pi$ and $E^2\Pi$, respectively, which is similar to the case of the ground state $X^2\Sigma^+$ in the Franck–Condon region.

3.3. Transition dipole moments and radiative lifetimes of SrH

The TDMs of several transitions to the ground $X^2\Sigma^+$ state and to the lowest excited states were calculated as the function of the internuclear distance, *R*, from 1.4 to 8 Å. The corresponding TDM curves for $A^2\Pi$–$X^2\Sigma^+$, $B^2\Sigma^+$–$X^2\Sigma^+$, $D^2\Sigma^+$–$X^2\Sigma^+$, $C^2\Sigma^+$–$X^2\Sigma^+$, $F^2\Sigma^+$–$X^2\Sigma^+$, $E^2\Pi$–$X^2\Sigma^+$, $^2\Pi(3)$–$X^2\Sigma^+$, $^2\Pi(4)$–$X^2\Sigma^+$ transitions are plotted in Fig. 6 and the TDM curves for excited state transitions are plotted in Fig. 7.

As shown in the upper panel of Fig. 5, in the Franck–Condon region (1.5–3.5 Å), the TDM of the $A^2\Pi$–$X^2\Sigma^+$ transition has the largest numerical value, which then reduces quickly to zero with increasing bond length. The calculated TDM curve is very similar to those determined by Gao et al. [27] and Leininger et al. [26]. The $B^2\Sigma^+$–$X^2\Sigma^+$ transition also has large values calculated for the TDM in this region and reaches a maximum at $R\sim3.3$ Å. However, large discrepancies are found with the results of Leininger et al. [26] especially in the 3.5–5 Å bond length range where the value obtained here is significantly less but peaks at a similar *R* value. Confirmation of the correct value for the TDM in this region will require new experimental work.

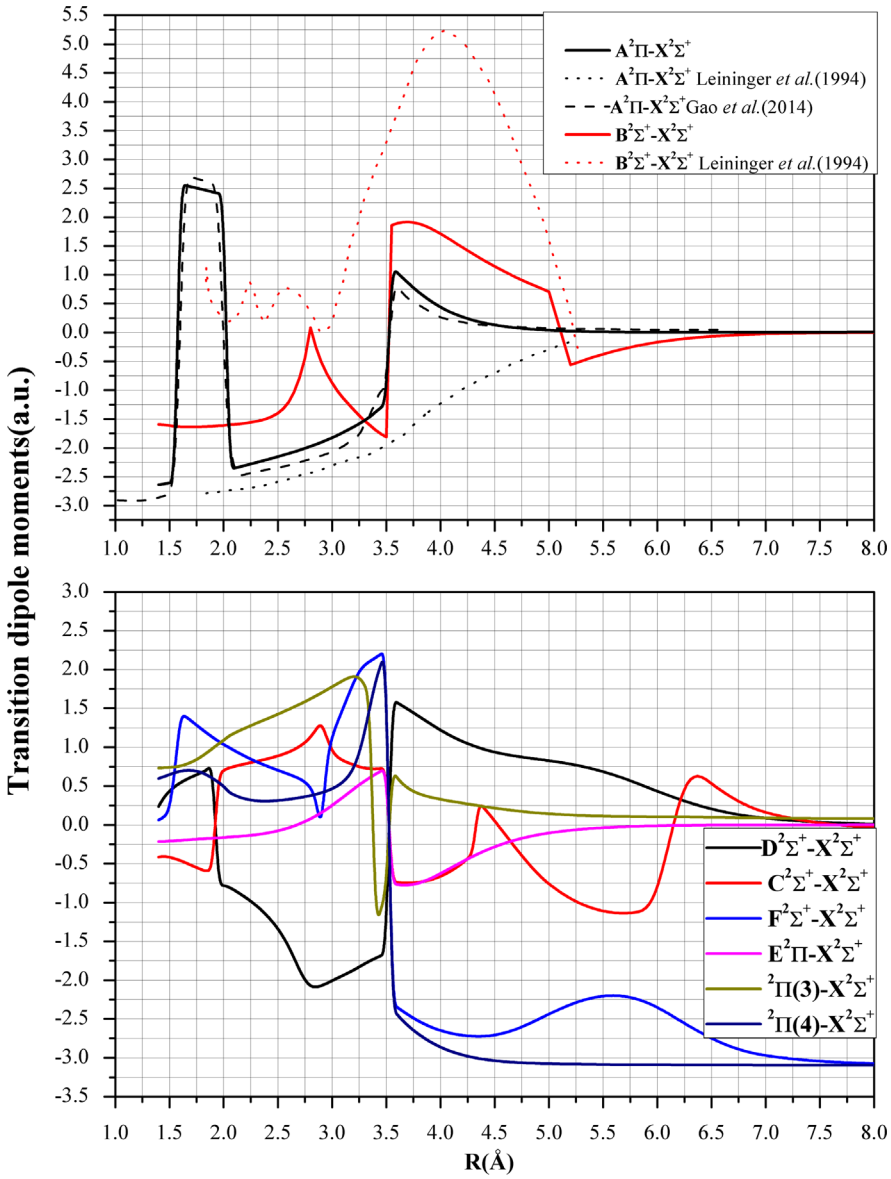

Fig. 6. The transition dipole moments of the selected transitions of SrH.

The TDMs of the transitions $^2\Pi(4)$–$X^2\Sigma^+$ and $F^2\Sigma^+$–$X^2\Sigma^+$ reach a large constant about −3a.u. at dissociation. The values correspond to TDMs of the spin-allowed transition ^1P_u–^1S_g for the Sr atom. In contrast, the remaining transitions are all associated with the spin-forbidden transitions, such as ^3P_u–^1S_g, ^3D_g–^1S_g, and ^1D_g–^1S_g for the Sr atom, and thus the TDMs tend to zero at large distance.

The Franck–Condon factors of the $A^2\Pi$–$X^2\Sigma^+$, $B^2\Sigma^+$–$X^2\Sigma^+$, $D^2\Sigma^+$–$X^2\Sigma^+$, $C^2\Sigma^+$–$X^2\Sigma^+$, $F^2\Sigma^+$–$X^2\Sigma^+$, $E^2\Pi$–$X^2\Sigma^+$, $^2\Pi(3)$–$X^2\Sigma^+$, $^2\Pi(4)$–$X^2\Sigma^+$, $E^2\Pi$–$A^2\Pi$, $D^2\Sigma^+$–$A^2\Pi$, $B^2\Sigma^+$–$A^2\Pi$, $A'^2\Delta$–$A^2\Pi$, $E^2\Pi$–$B^2\Sigma^+$, $D^2\Sigma^+$–$B^2\Sigma^+$ and $E^2\Pi$–$A'^2\Delta$ transitions are calculated with the aid of the LEVEL program [30] and listed in Table S1. The Franck-Condon factors of $A^2\Pi$–$X^2\Sigma^+$, $B^2\Sigma^+$–$X^2\Sigma^+$, $C^2\Sigma^+$–$X^2\Sigma^+$, $E^2\Pi$–$X^2\Sigma^+$, $E^2\Pi$–$A^2\Pi$, $E^2\Pi$–$B^2\Sigma^+$ and $E^2\Pi$–$A'^2\Delta$ systems of SrH indicate that the $\Delta\nu$ (ν'-ν'')=0 bands are more intense than the other bands. This is due to the $X^2\Sigma^+$, $A^2\Pi$, $B^2\Sigma^+$, $C^2\Sigma^+$, $E^2\Pi$, and $A'^2\Delta$ states having similar equilibrium internuclear distances.

For the aforementioned transitions, the radiative lifetimes of selected vibrational levels, ν', have been computed by the following formula [42,43].

$$\tau_{\nu'} = (A_{\nu'})^{-1} = \frac{3h}{64\pi^4 |a_0 \times e \times TDM|^2 \Sigma_{\nu''} q_{\nu',\nu''} (\Delta E_{\nu',\nu''})^3}$$

$$= \frac{4.936 \times 10^5}{|TDM|^2 \Sigma_{\nu''} q_{\nu',\nu''} (\Delta E_{\nu',\nu''})^3} \quad (2)$$

where $q_{\nu',\nu''}$ is the Franck–Condon factor (FCF); TDM is averaged transition dipole moment in atomic units (a.u.), which is substituted with single-point TDM at the equilibrium of the lower states in present work; ΔE is the energy difference

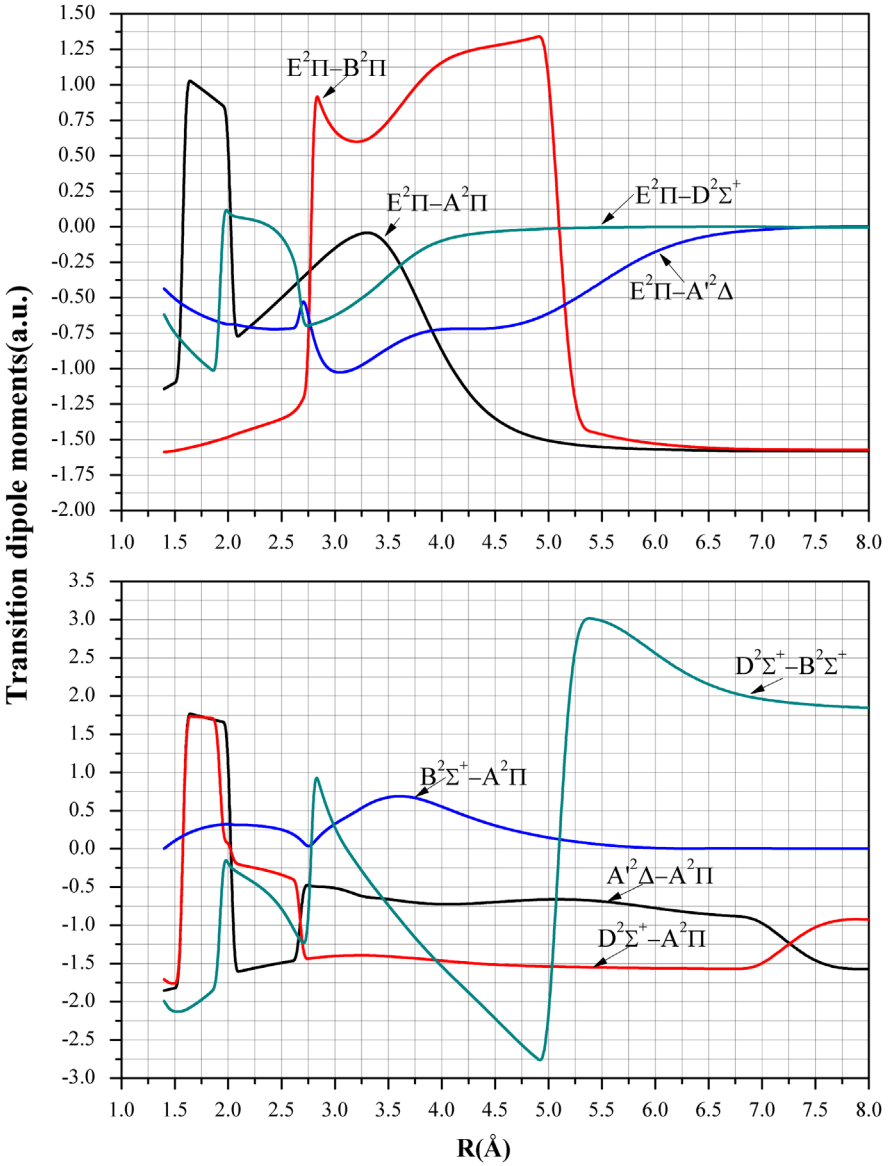

Fig. 7. The transition dipole moments of excited state transitions of SrH.

between vibrational levels ν' and ν''; τ is in second. The radiative lifetimes of the aforementioned transitions are listed in the Table 4. Calculated values 34.2 ns ($\nu'=0$) and 33.9 ns ($\nu'=1$) of the radiative lifetimes for the $A^2\Pi$–$X^2\Sigma^+$ transition, are in good agreement with the experimental values 33.2 ± 3.2 ns and 33.7 ± 5.3 ns and the theoretical results calculated by Gao et al. [27]. Considering the spin–orbit coupling effect, we have also calculated the radiative lifetimes of the $A^2\Pi_{1/2}$–$X^2\Sigma^+_{1/2}$ and $A^2\Pi_{3/2}$– $X^2\Sigma^+_{1/2}$ transitions, which the values are 36.5 ns and 34.9 ns and are in accordance with the experimental value 33.8 ± 1.9 ns and 32.3 ± 2.0 ns [23]. The predicted radiative lifetimes values for the $B^2\Sigma^+$–$X^2\Sigma^+$ are 55.0 ns ($\nu'=0$) and 54.7 ns ($\nu'=1$) and are compared with the known experimental data of 48.4 ± 2.0 ns ($\nu'=0$) and 50.5 ± 3.2 ns ($\nu'=1$) [23].

4. Conclusion

High-level icMRCI+Q calculations have been performed to calculate the PECs of the 16 Λ–S states of SrH. From the PECs of the bound states, the corresponding spectroscopic constants are determined by solving the radial Schrödinger equation, and found to be in good agreement with previous experimental measurements. The calculated PECs also show the high state density of the SrH molecule. The most important of which is the four strongly bound states including the $A^2\Sigma^+$, $A'^2\Delta$, $B^2\Pi$, and $D^2\Sigma^+$ that are calculated to lie close in energy to each other. The spin–orbit matrix elements indicate that strong interactions exist in the $X^2\Sigma^+$–$A^2\Pi$, $B^2\Sigma^+$–$A^2\Pi$, and $D^2\Sigma^+$–$A^2\Pi$ systems. SOC splits the $X^2\Sigma^+$, $A^2\Pi$, $A'^2\Delta$, $B^2\Sigma^+$, and $D^2\Sigma^+$ states into 9 Ω states. The calculated splitting between the $\Omega=1/2$ and 3/2 components of the $A^2\Pi$ state of 248 cm^{-1} reproduces the previous theoretical value

Table 4
The radiative lifetimes of the selected transitions of the SrH molecule.

Transition		Radiative lifetime				
		$\nu'=0$	$\nu'=1$	$\nu'=2$	$\nu'=3$	$\nu'=4$
$A^2\Pi$–$X^2\Sigma^+$	(ns)	34.2	33.9	33.5	33.2	32.9
Expt.		33.8 ± 1.9[a]/33.2 ± 3.2[b]	33.7 ± 5.3[b]			
Calc.		33.2[c]	33.3[c]	33.8[c]	33.6[c]	33.8[c]
$A^2\Pi_{1/2}$–$X^2\Sigma^+_{1/2}$		36.5				
Expt.		33.8 ± 1.9[b]				
$A^2\Pi_{3/2}$–$X^2\Sigma^+_{1/2}$		34.9				
Expt.		32.3 ± 2.0[b]				
$B^2\Sigma^+$–$X^2\Sigma^+$	(ns)	55.0	54.7	54.5		
Expt.		48.4 ± 2.0[b]	50.5 ± 3.2[b]			
$D^2\Sigma^+$–$X^2\Sigma^+$	(ns)	129	112	104	99.9	98.2
$C^2\Sigma^+$–$X^2\Sigma^+$	(ns)	42.2	41.0	40.1	39.3	38.8
$F^2\Sigma^+$–$X^2\Sigma^+$	(ns)	195	172	171		
$E^2\Pi$–$X^2\Sigma^+$	(μs)	3.06	3.08	3.11	3.14	3.19
$^2\Pi(3)$–$X^2\Sigma^+$	(ns)	16.1	25.0	26.0	36.5	38.6
$^2\Pi(4)$–$X^2\Sigma^+$	(ns)	14.1	12.6	13.5	15.0	20.1
$E^2\Pi$–$A^2\Pi$	(μs)	4.38	4.52	4.69	4.91	5.20
$D^2\Sigma^+$–$A^2\Pi$	(μs)	42.9	16.1	9.45	7.39	6.18
$B^2\Sigma^+$–$A^2\Pi$	(μs)	5610	5950	6360	7660	
$A'^2\Delta$–$A^2\Pi$	(μs)	4.74	4.93	5.09	5.34	5.67
$E^2\Pi$–$B^2\Sigma^+$	(μs)	1.96	2.01	2.07	2.11	260
$D^2\Sigma^+$–$B^2\Sigma^+$	(μs)	11.9	3.97	2.15	1.55	1.30
$E^2\Pi$–$A'^2\Delta$	(μs)	70.9	67.8	67.2	68.5	69.5

[a] Ref [22].
[b] Ref [23].
[c] Ref [27].

of 233 cm^{-1}. The SOC also leads to the elevation of the potential well and the shortening of the bond length for the $D^2\Sigma^+$ state. The TDMs, Franck–Condon factors, and radiative lifetimes are determined. The lifetimes are calculated to be 34.2 ns ($\nu'=0$), 36.5 ns ($\nu'=0$), 34.9 ns ($\nu'=0$) and 55.0 ns ($\nu'=0$) for $A^2\Pi$–$X^2\Sigma^+$, $A^2\Pi_{1/2}$–$X^2\Sigma^+_{1/2}$, $A^2\Pi_{3/2}$–$X^2\Sigma^+_{1/2}$ and $B^2\Sigma^+$–$X^2\Sigma^+$ states, in good agreement with the experimental results of 33.8 ± 1.9 ns, 33.8 ± 1.9 ns, 32.3 ± 2.0 ns and 48.4 ± 2.0 ns. The calculated results reported with revealing the more details about the structure and behavior of the low-lying electronic states of the SrH molecule.

Acknowledgment

This work was supported by National Natural Science Foundation of China (Grant Nos. 11574114, U1532138, 11474032 and 11274140) and Natural Science Foundation of Jilin Province (Grant No. 20150101003JC).

Appendix A. Supplementary material

Supplementary data associated with this article can be found in the online version at http://dx.doi.org/10.1016/j.jqsrt.2015.11.001.

References

[1] Dai DG, Balasubramanian K. Spectroscopic constants and potential energy curves of IrH. New J Chem 1991;15:721–6.
[2] Stwalley WC, Zemke WT, yang SC. Spectroscopy and structure of the alkali hydride diatomic molecules and their ions. J Phys Chem 1991;20:153–87.
[3] Yang XZ, Lin MR, Zou WL, Zhang BZ. Ab initio study on the ground and low-lying excited states of GaH. Chem Phys Lett 2003;372:355–61.
[4] Zou WL, Liu WJ. Theoretical study on the low-lying electronic states of NiH and NiAt. J Comput Chem 2007;28:2286–98.
[5] Li R, Zhang XM, Jin MX, Yan B, Xu HF. Theoretical investigation of potential energy curves and radiative lifetimes of low-lying electronic states in GeH^+ radical cation. Chem Phys Lett 2014;594:6–12.
[6] Zhang XM, Liang GY, Li R, Shi DD, Liu YC, Liu XS, et al. Multi-reference configuration interaction study on the potential energy curves and radiative lifetimes of low-lying excited states of CdH^+ cation. Chem Phys 2014;443:142–8.
[7] Huang HY, Chang YY, Liao MH, Wu KL, Lu TL, Chang YY, et al. Characterization of the outer well of NaH $C^1\Sigma^+$ state by fluorescence depletion spectroscopy. Chem Phys Lett 2010;493:53–6.
[8] Li R, Zhai Z, Zhang XM, Jin MX, Xu HF, Yan B. Spin–orbit all-electron configuration interaction study on the electronic structure and radiative lifetimes of low-lying excited states of CdH. Chem Phys Lett 2014;599:51–6.
[9] Li R, Zhai Z, Zhang X, Jin M, Xu H, Yan B. All-electron spin–orbit configuration interaction study on the valence and low-lying Rydberg electronic states of GeH. J Quant Spectrosc Radiat Transfer 2015;157:42–53.
[10] Yadin B, Veness T, Conti P, Hill C, Yurchenko SN, Tennyson J. ExoMol line lists-I. The rovibrational spectrum of BeH, MgH and CaH in the $X^2\Sigma^+$ state. Mon Not R Astron Soc 2012;425:34–43.
[11] Sotirovski P. The molecular spectrum of sunspot umbrace. Astron Astrophys 1971;14:319–36.
[12] Sakamoto S, White GJ, Kawaguchi K, Ohishi M, Usuda KS, Hasegawa T. A search for absorption of Mg and Ca compounds in molecular clouds towards Galactic continuum sources. Mon Not R Astron Soc 1998;301:1872–80.
[13] Pitarch-Ruiz J, Sanchez-Marin J, Velasco AM. Full configuration interaction calculation of the low lying valence and Rydberg states of BeH. J Comput Chem 2008;29:523–32.
[14] Kaupp M, PvR Schleyer, Stoll H, Preuss H. Pseudopotential approaches to Ca, Sr, and Ba hydrides. Why are some alkaline earth MX_2 compounds bent? J Chem Phys 1991;94:1360–6.

[15] Lim IS, Stoll H, Schwerdtfeger P. Relativistic small-core energy-consistent pseudopotentials for the alkaline-earth elements from Ca to Ra. J Chem Phys 2006;124:034107.
[16] Lin K-C, Ureña AG. Dynamical and stereodynamical studies of alkaline-earth atom-molecule reactions. Int Rev Phys Chem 2007;26:289–352.
[17] Lambert DL, Warner B. The abundances of the elements in the solar photosphere. Mon Not R Astron Soc 1968;138:181–212.
[18] Sauval AJ, Tatum JB. A set of partition functions end equilibrium constants for 300 diatomic molecules of astrophysical interest. Astrophys J Suppl Ser 1984;56:193–209.
[19] Ramachandran PS, Rajamanickam N, Bagare SP. Evaluation of astrophysically useful parameters for strontium monohydride and deuteride. Serb Astron J 2006;172:13–6.
[20] Watson WW, Fredrickso WR. The spectrum of strontium hydride. Phy Rev 1932;39:765–76.
[21] Appelblad Klynning L. Fourier transform spectroscopy of SrH: the A–X and B–X band systems. Phys Scr 1986;33:415–9.
[22] Berg L-E, Ekvall K, Hishikawa A, Kelly S, McGuinness C. Laser spectroscopy of SrH. Time-resolved measurements of the $A^2\Pi$□state. Chem Phys Lett 1996;255:419–24.
[23] Pauchard T, Liu M, Launila O, Berg LE. Time-resolved studies of the $A^2\Pi$ and $B^2\Sigma^+$ states of SrH by laser spectroscopy. J Mol Spectrosc 2008;247:181–3.
[24] Shayesteh A, Walker KA, Gordon I, Appadoo DRT, Bernath PF. New Fourier transform infrared emission spectra of CaH and SrH: combined isotopomer analyses with CaD and SrD. J Mol Struct 2004;695–696:23–37.
[25] Ram RS, Tereszchuk K, Walker KA, Bernath PF. High resolution emission spectroscopy of the $E^2\Pi$–$X^2\Sigma^+$ transition of SrH and SrD. J Mol Spectrosc 2012;271:15–9.
[26] Leininger T, Jeung G-H. Calculation of double-well B vibronic states of SrH. Phys Rev A 1994;49:2415–20.
[27] Gao YF, Gao T. Laser cooling of the alkaline-earth-metal monohydrides: Insights from anab initiotheory study. Phys Rev A 2014;90:052506.
[28] Werner H, Knowles P, Knizia G, Manby FR, Schütz M, Celani P, et al. Molpro, version 2010.1, a package of ab initio programs 2010.
[29] Werner HJ, Knowles PJ, Knizia G, Manby FR, Schütz M. Molpro: a general-purpose quantum chemistry program package. WIREs Comput Mol Sci 2012;2:242–53.
[30] Le Roy R. LEVEL 8.0: A computer program for solving the radial Schrödinger equation for bound and quasibound levels. University of Waterloo Chemical Physics Research Report CP-663 2007.
[31] Li HD, Feng H, Wi Sun, Zhang Y, Fan QC, Peterson KA, et al. The alkaline earth dimer cations (Be_2^+, Mg_2^+, Ca_2^+, Sr_2^+, and Ba_2^+). Coupled cluster and full configuration interaction studies. Mol Phys 2013;111:2292–8.
[32] Thom H, Dunning J. Gaussian basis sets for use in correlated molecular calculations. I. The atoms boron through neon and hydrogen. J Chem Phys 1989;90:1007–23.
[33] Werner HJ, Meyer W. A quadratically convergent multiconfiguration-self-consistent field method with simultaneous optimization of orbitals and CI coefficients. J Chem Phys 1980;73:2342–56.
[34] Werner HJ, Knowles PJ. A second order multiconeuration SCF procedure with optimum convergence. J Chem Phys 1985;82:5053–63.
[35] Langhoff SR, Davidson ER. Configuration interaction calculations on the nitrogen molecule. Int J Quantum Chem 1974;8:61–72.
[36] Moore CE. Atomic Energy Levels. Washington, DC: National Bureau of Standards; 1971.
[37] Huber KP, Herzberg G. Molecular Structure and Molecular Spectra IV: Constants of Diatomic Molecules. New York: Van Rostrand-Reinhold; 1979.
[38] Korek M, Razzouk H, Arkoub RA, Atwani SE. The low-lying excited electronic states of an alkali-earth compounds. Adv Mater Res 2011;324:282–5.
[39] More KR, Corṅell SD. The band spectra of SrCl and SrH. Phys Rev 1938;53:806–11.
[40] Yang XZ, Boggs JE. Extensive ab initio study of the valence and low-lying Rydberg states of BBr including spin–orbit coupling. J Chem Phys 2006;124:194307.
[41] Khalil H, Le Quéré F, Brites V, Léonard C. Theoretical study of the rovibronic states of CaO. J Mol Spectrosc 2012;271:1–9.
[42] Okabe H. Photochemistry of Small Molecules. New York: Wiley-Interscience; 1978.
[43] Zou WL, Liu WJ. Extensive theoretical studies on the low-lying electronic states of indium monochloride cation, $InCl^+$. J Comput Chem 2005;26:106–13.